High-performance calculation of the acoustic backscattering strength based on the Kirchhoff high-frequency approximation

Ralf Burgschweiger[a], Ingo Schäfer[b], Delf Sachau[a], Jan Ehrlich[b]

[a] Helmut Schmidt University, University of the Federal Armed Forces Hamburg (UniBw/H), Faculty of Mechanical Engineering, Chair of Mechatronics
[b] Bundeswehr Technical Center for Ships and Naval Weapons, Maritime Technology and Research (WTD71), Acoustic Modeling (GF640)

Ralf Burgschweiger, Helmut Schmidt University, Faculty of Mechanical Engineering, Holstenhofweg 85, 22043 Hamburg, Germany
Tel. +49-30-45 80 36 84
Email: burgschr@hsu-hh.de

Abstract: *The acoustic backscatter strength (target echo strength, TES) of underwater objects, which is important for sonar applications, can be determined by different numerical methods (boundary element method, finite element method, ray tracing and approximate methods). These are capable of considering taking into account both the hull and, to some extent, the internal structures of the object under consideration, although the computational effort required increases significantly with higher complexity. In order to make a fast prediction for the radiation behavior of mostly concave objects, e.g., the outer hull of a submarine, the Kirchhoff high-frequency approximation (KIA) method has been widely used since the middle of the last century, which uses optical analogies and is primarily suitable for high frequencies. The extension of the instruction sets of current CPUs allows the parallel execution of floating-point operations (Advanced Vector Extensions) with 8 or 16 real numbers within one machine instruction. In the context of the research project "Computational Acoustics", an existing conventional code was optimized accordingly using the AVX2 variant. In this presentation, the fundamentals, results, and computation times for a very fast variant of the Kirchhoff high-frequency approximation (KIA) are presented and compared with results of other methods.*

Keywords: *Kirchhoff approximation, Target echo strength, High performance calculation, Advanced vector extensions*

1. INTRODUCTION

The acoustic backscattering strength (target echo strength, TES) corresponds to the ratio of incident to reflected sound intensity [1]. In order to obtain comparable values, a sound source is placed in the far field of the object and then the backscattering strength is determined, which is calculated back to a distance of one meter from the object.

The boundary element method (BEM) is suitable for this purpose, since the sound field reflected by the object to be examined should in theory be a free field. Accordingly, only the surface of the object itself must be discretized. Here, the rule of thumb, which states that at least six elements per wavelength should be used, should be observed.

The computational effort therefore increases extremely for high frequencies (more than 300 kHz occur in sonar technology). Significant runtime reduction can be achieved by various high-frequency approximations. One way to circumvent the rule of thumb using arbitrary coarse surface elements that depend only on the geometry of the object of interest was described in [2]. This method can be further accelerated using current CPU technologies whose instruction sets allow parallel execution of floating-point operations (Advanced Vector Extensions, [3]) with 8 or 16 real numbers of single precision within one machine instruction.

2. BASIC FORMULATION

The backscattered pressure from the object using the Kirchhoff method for the monostatic case is formed according to the following formula (full details see [2], eqns. (2) … (7)):

$$p_s \approx \frac{p_0}{2\pi} \iint_{\Gamma_{ill}} \frac{R\mathrm{e}^{-i2k|\vec{s}|}}{|\vec{s}|^4} (ik|\vec{s}| + 1)\vec{s} \cdot \vec{n}\, \mathrm{d}\Gamma \tag{1}$$

with

$\vec{e}_c$	Center of the element
$\vec{e}_n$	n. vertex (corner point) of the element ($n = 1 \ldots 3$)
p_s	backscattered sound pressure
p_0	Amplitude of the incident sound pressure
R	Reflection coefficient (complex), frequency and angle dependent
k	frequency dependent wave number ($k = c/f$)
$\vec{r}$	Source = evaluation point (for monostatic calculation)
$\vec{r}_0$	normalized vector of $\vec{r}$
$\vec{s}$	Distance vector between element center and source point ●
$\vec{n}$	Normal vector of the element
Γ_{ill}	"Illuminated" part of the surface

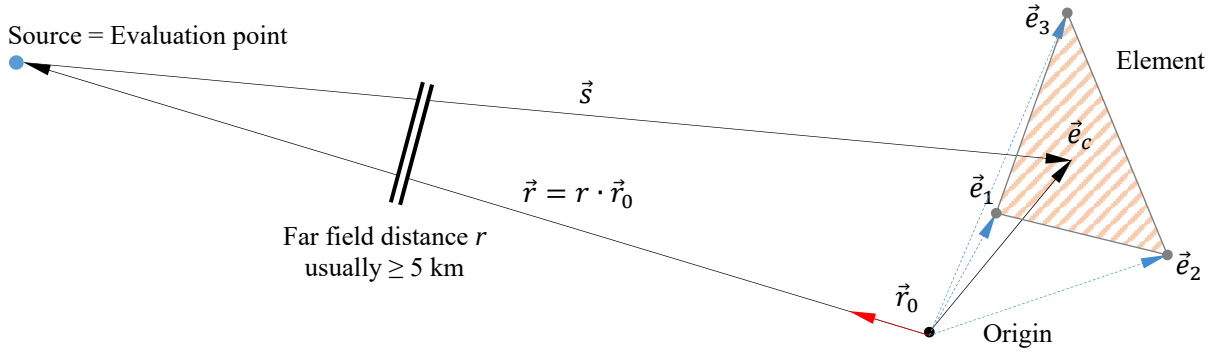

Fig. 1: Backscattering for one triangle (vector scheme for the monostatic case)

Due to the large distance between element and evaluation point (far field conditions), the vectors $\vec{r}$ and $\vec{s}$ are nearly parallel in the monostatic case.

In order to perform the integration according to Eq. (1), the triangle must be parameterized. The necessary parameters for this are λ and μ, they run through the values from 0 ... 1.

Using the approximations described in [2], eqns. (8) to (10), lead to the following integral equation for the monostatic case:

$$p_s \approx \frac{ikRp_{inc}}{2\pi r^3} \iint_{\Delta} \mathrm{e}^{-i2k(r-\vec{e}_1\cdot\vec{r}_0-(c_1-\lambda\mu c_2)}(\vec{r}_0\cdot\vec{n})\lambda\,\mathrm{d}\lambda\,\mathrm{d}\mu \tag{2}$$

Eq. (2) describes the backscatter strength for an "illuminated" triangle at an arbitrarily high frequency and gives the following concrete formulation per surface element after discretization:

$$p_s = \frac{p_{inc}\mathrm{e}^{i2kr}}{i8\pi r^3} \cdot \frac{R(\vec{r}_0\cdot\vec{n})\mathrm{e}^{i2k\vec{e}_1\cdot\vec{r}_0}}{c_2} \cdot \left[\frac{\mathrm{e}^{i2k(c_1+c_2)}-1}{c_1+c_2} - \frac{\mathrm{e}^{i2kc_1}-1}{c_1}\right] \tag{3}$$

with $c_1 = (\vec{e}_2-\vec{e}_1)\cdot\vec{r}_0,\ c_2 = (\vec{e}_3-\vec{e}_2)\cdot\vec{r}_0$

2.1. Optimizations implemented

In Eq. (3), 4 scalar products (marked red) and 6 sine or cosine calculations (from the complex exponential functions, marked green) are required per element. To achieve the best computational performance using AVX2 intrinsics [3], the following practices were implemented:

a) Re-sorting of all used geometric parameters into separate X, Y and Z fields
b) Pre-calculation of all occurring complex reflection factors and indexed access depending on the incident angle
c) Blockwise multithreaded calculation of all requested field points for 8 elements at a time (the AVX2 commands can process 8 single precision values simultaneously)
d) Fast computation of $\frac{(\mathrm{e}^{ix}-1)}{x} = \frac{\cos(x)-1}{x} + i\frac{\sin(x)}{x}$ by an optimized AVX2-based function
e) Optimal utilization of the CPU cache through block-adapted memory access

3. MODEL USED

The outer hull of the BeTSSi [4] model (Fig. 2), consisting of 178,000 or 713,000 triangular elements, was used as the test structure. The dimensions are 60 × 11 × 7 m³ (W×H×D).

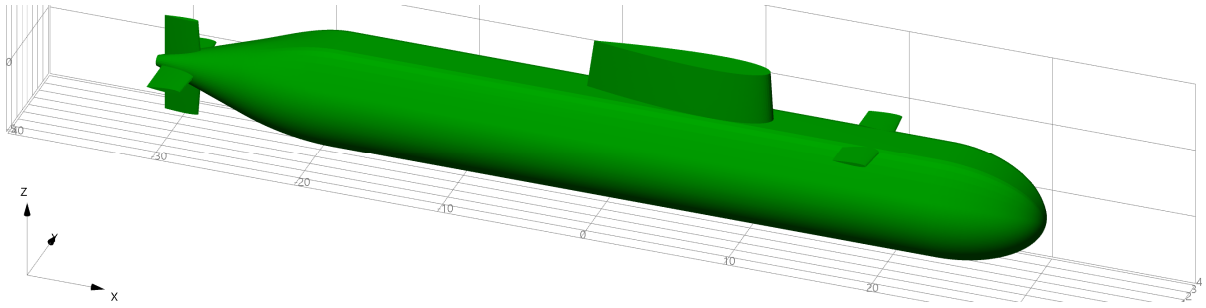

Fig. 2: BeTSSi model (outer hull only)

This model contains convex parts e.g. at the rudders. These can cause multiple reflections. Therefore, differences of alternative solution methods can be recognized.

4. RESULTS

For all calculations in this publication, a rigid boundary condition was specified in order to keep the solution times within reasonable limits, although other conditions may also be used (reflection coefficients, shells [5], etc.) depending on the solution method applied.

For the comparisons, all calculations were performed on the same workstation (AMD EPYC, 3.2 GHz, 32 cores, 64 threads, 512 GB main memory) under MS Windows 10 Prof. (64 bit).

4.1. Surface pressure and bistatic target echo strength (f = 3 kHz)

To illustrate the differences in the pressure profile between different methods, fig. 3 show its real part $\Re(p_s)$ on the surface of the finer discretized model at a frequency f = 3 kHz (sound incidence at α_{asp} = 55°, α_{elev} = 10°, see arrow), the range of values shown covers ± 3 N/m².

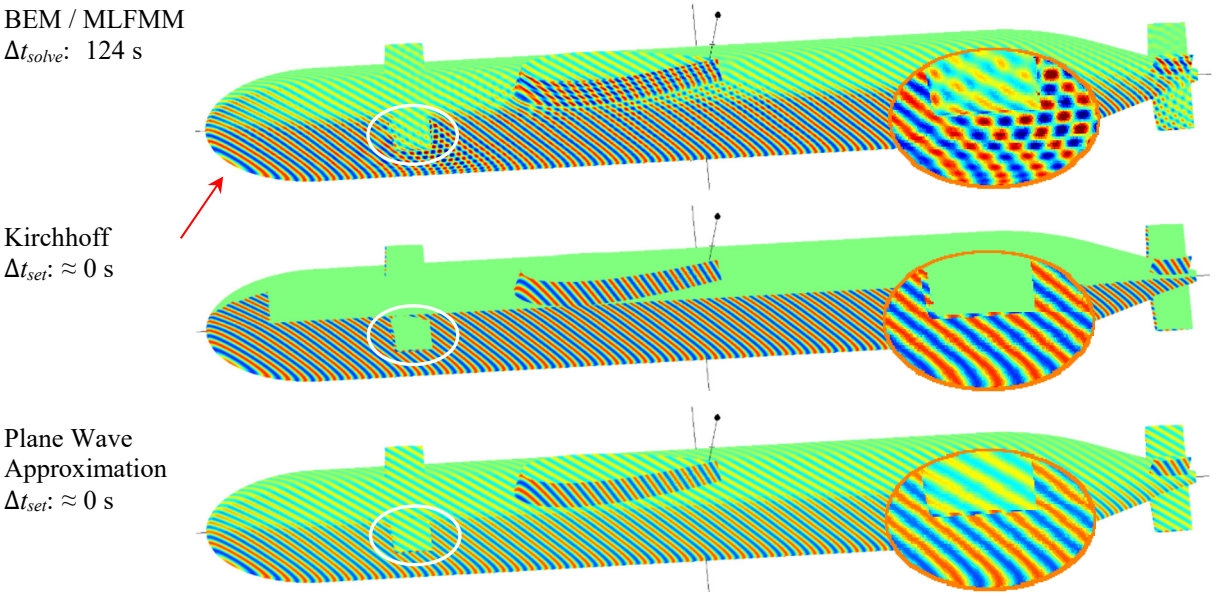

Fig. 3: Surface pressure $\Re(p_s)$ for the BEM, KIA and PWA, f = 3 kHz

The matrix-based BEM solution represents the "reference" and was calculated using the Multi-Level Fast Multipole Method (MLFMM, [6]) due to the size of the problem. Since the pressure is only set in the approximation methods, this time cost (Δt_{set}) can be neglected.

With the Kirchhoff solution, the "unilluminated" elements are clearly visible, while in the plane-wave approximation (PWA, [7]) the pressure pattern is smoother but has a slightly lower amplitude. The differences within the pressure profile in the areas with reflections (under the front rudder, at the tower and the rear rudder) between the BEM and the approximation methods are clearly visible in the enlarged sections.

Fig. 4 shows the polar pattern of the bistatic TES based on the results given above.

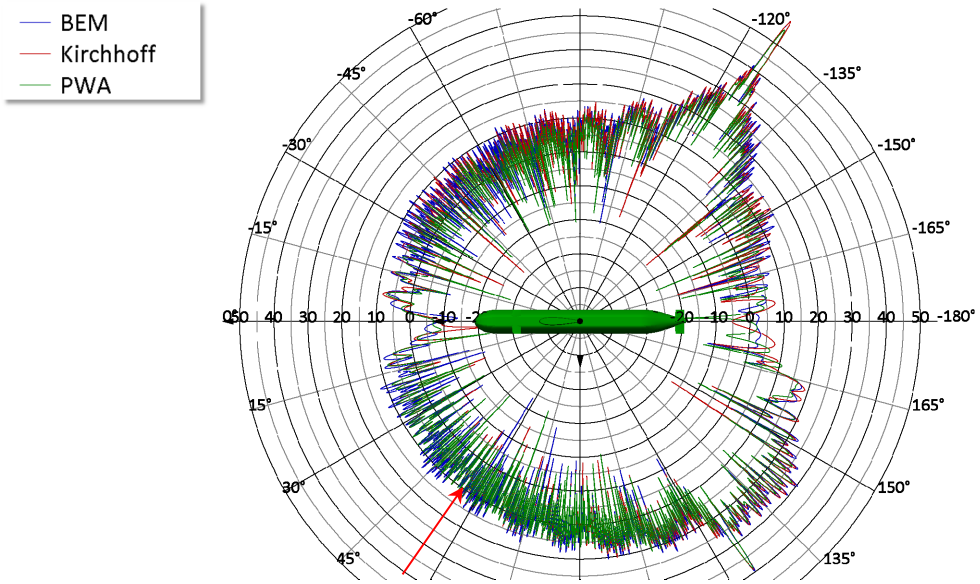

Fig. 4: TES, bistatic, f = 3 kHz, α_{asp} = 55°, circle, XY plane (0.2° steps, 1.801 points)

Despite the differences in the pressure profile on the surface, the TES profiles agree well, only the PWA is slightly lower within the maxima.

4.2. Target echo strength (monostatic, f = 1 kHz, semi-circle, 180°)

Figs. 5 and 6 show the results of monostatic calculations for the frequency f = 1 kHz (wave length λ = 1.5 m, $\lambda/6$ = 0.25 m) in the XY plane (0° ... 180°, step width 0.1°, 1,801 evaluation points). The variant with 178,000 elements was used (edge length: approx. 0.14 m) to allow a monostatic BEM calculation with multiple right sides (memory requirement: approx. 243 GB).

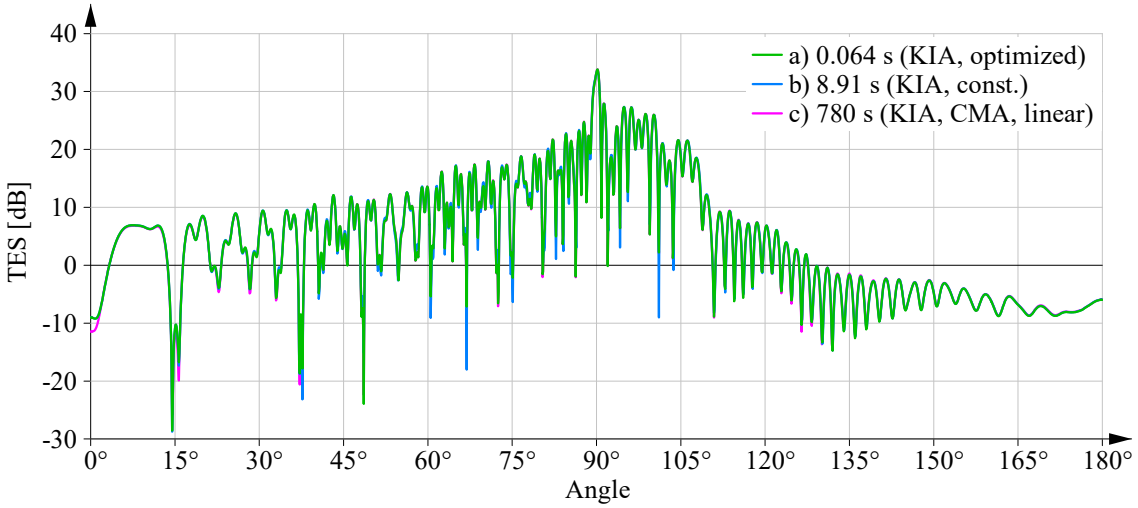

Fig. 5: TES, monostatic, Kirchhoff methods only, f = 1 kHz

In comparing the three Kirchhoff-based methods, the plots are almost identical, but the differences between the solution times are significant. For the third solution (CMA), which was calculated with a commercial application, linear approach functions were used for the integration and thus significantly more computing time was required.

Comparing the results from the BEM and our ray tracing method (Fig. 6, [8]), the results differ somewhat more, especially in the “quieter” range between 135° and 180° and around 0°, but still well usable.

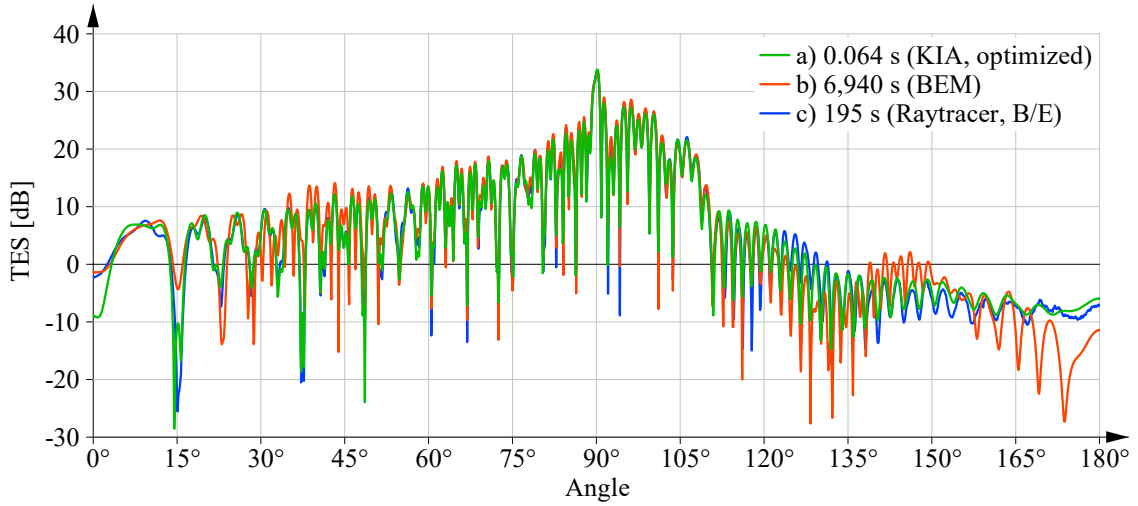

Fig. 6: TES, monostatic, comparison with BEM and ray tracer, f = 1 kHz

However, it should be noted that the solution time for the "reference solution" BEM is comparatively very high. Table 1 shows the factors for the required computation times, related to the optimized Kirchhoff variant.

Kirchhoff optimized	Kirchhoff	Raytracer	Kirchhoff CMA lin.	BEM
1	140	3,050	12,200	108,000

Table 1: Factors of the computation time, f = 1 kHz

4.3. Target echo strength (monostatic, f = 8 kHz, semi-circle, 180°)

Figs. 7 and 8 represent the results of monostatic calculations for the frequency f = 8 kHz (wavelength λ = 0.188 m, $\lambda/6$ = 0.032 m). At this frequency, the rule of thumb "six elements per wavelength" is violated (edge length: approx. 0.14 m), so that the pressure gradients per element can no longer be reproduced precisely and the results are therefore inaccurate.

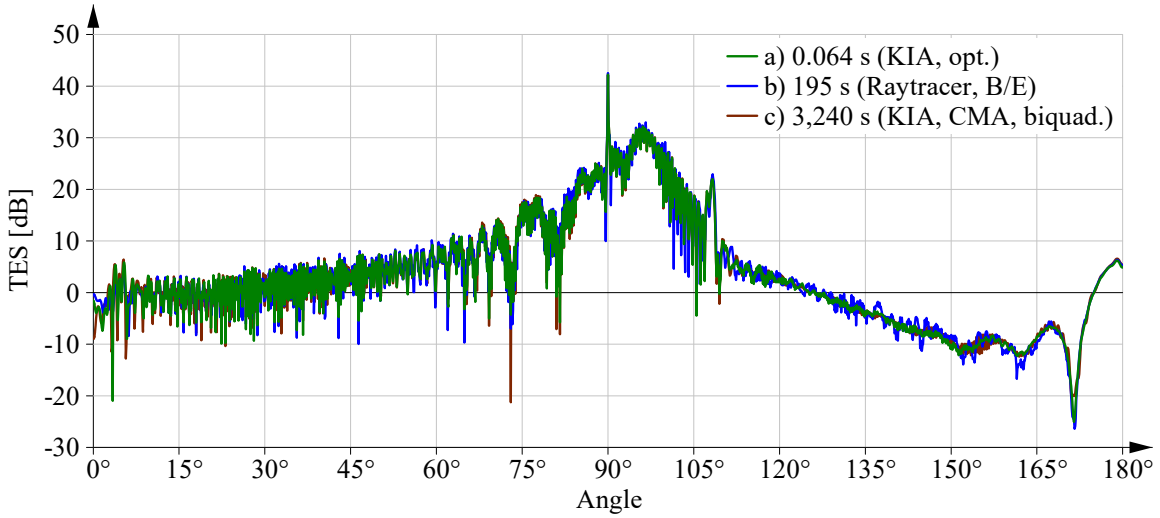

Fig. 7: TES, monostatic, f = 8 kHz, applicable solutions

The comparison between the optimized KIA, the raytracer and the commercial application also shows a very good agreement here.

However, in the commercial application (CMA), biquadratic approach functions had to be selected in order to obtain a qualitatively comparable result with the edge length used. The optimized KIA method has no problems here yet.

Fig. 8 gives the results of the other available solution methods.

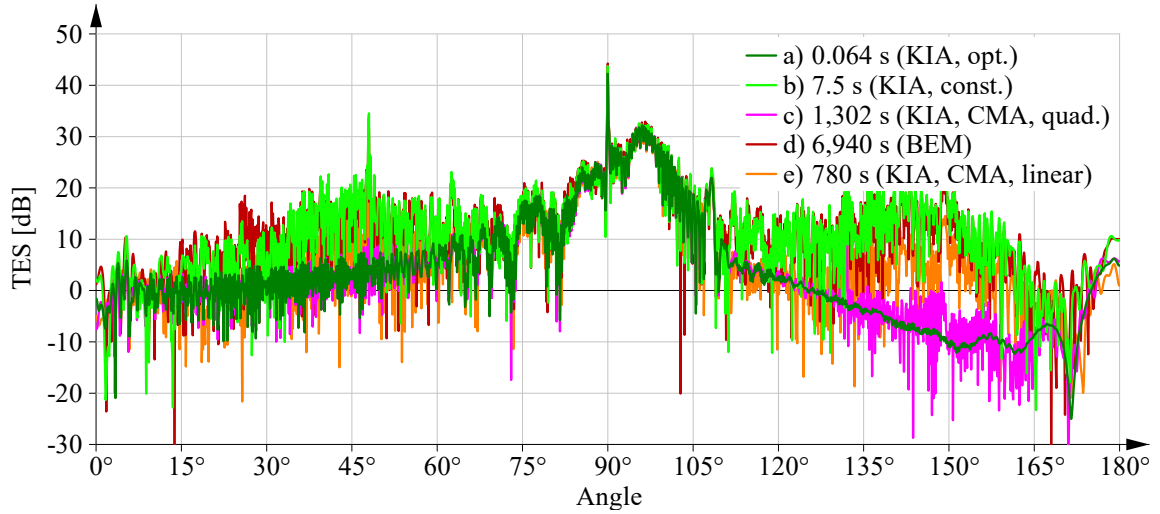

Fig. 8: TES, monostatic, f = 8 kHz, other solutions

It is clearly visible that the solutions of these methods are no longer usable for this higher frequency, since they provide insufficient results. Table 2 shows the factors for the required computation times at f = 8 kHz.

Kirchhoff optimized	Kirchhoff	Raytracer	Kirchhoff CMA lin.	Kirchhoff CMA quad.	Kirchhoff CMA biquad.	BEM
1	120	3,050	12,200	20,300	50,625	108,000

Table 2: Factors of the computation time, f = 8 kHz

4.4. Target echo strength (monostatic, spherical section, averaged)

Finally, the results of monostatic calculations for a spherical section (α_{asp} = 0°...180°, α_{elev} = ± 20°, step width 0.2°) will be shown. The calculations were performed for 11 frequencies (f = 2.7 … 3.3 kHz) and the results given were averaged for all 181,101 evaluation points.

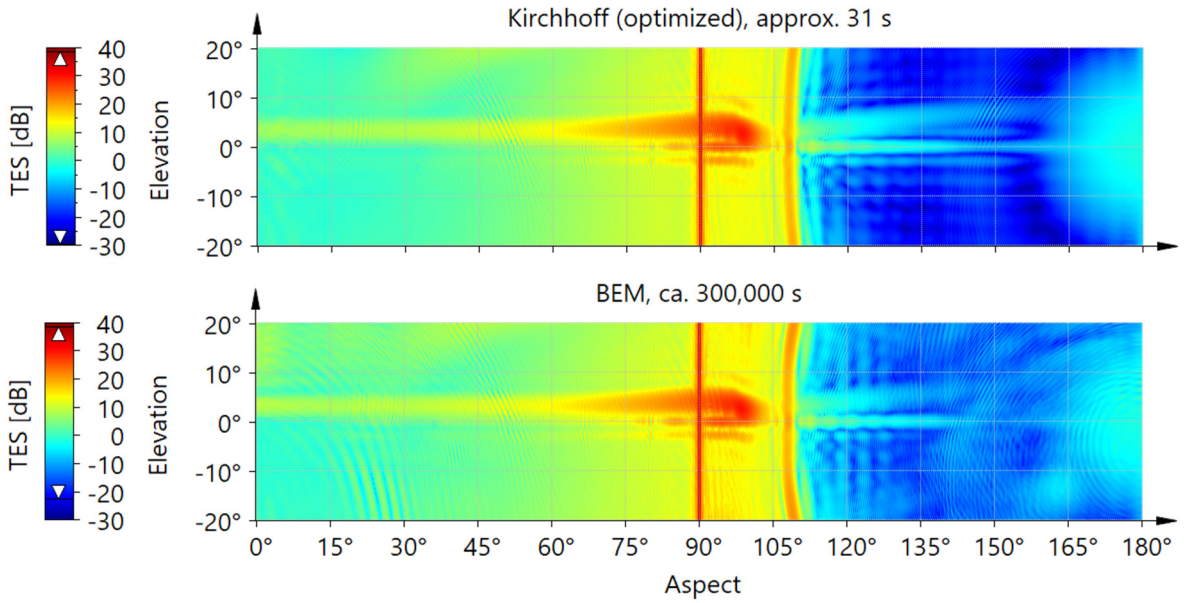

Fig. 9: TES, spherical section, f_{aver} = 3 kHz, KIA and BEM, averaged over 11 frequencies

The qualitative and quantitative agreement of both results in the relevant areas is surprisingly good and has only small differences in the regions with low backscatter strength. The calculation times with a factor of approx. 10,000 speak for themselves.

For clarification, Fig. 10 shows the TES pressure profile in the far field on the imaging surface used.

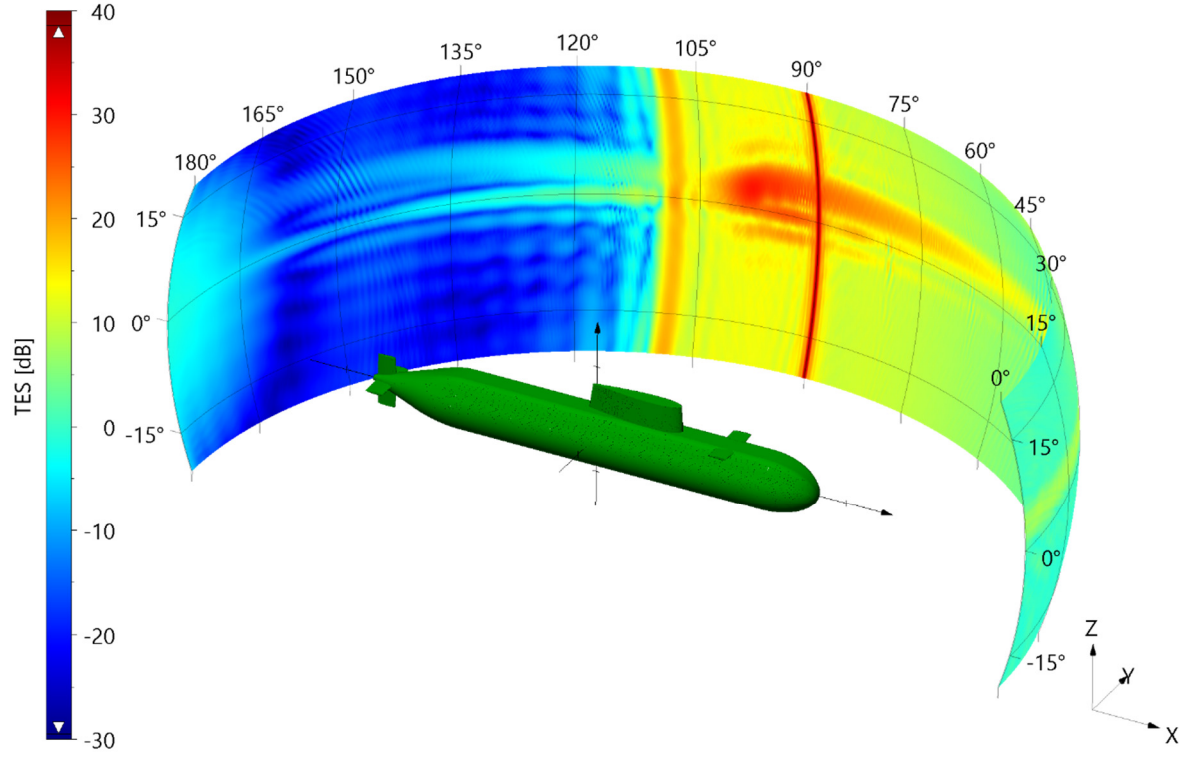

Fig. 10: TES, spherical section, f_{aver} = 3 kHz, KIA, averaged over 11 frequencies 3D projection

5. SUMMARY AND OUTLOOK

This paper illustrates the advantages that can be achieved by re-evaluating and optimizing "older" solution methods.

The performance of the optimized AVX-Kirchhoff variant clearly outperforms the "conventional" variant with identical computational results and shows good to very good quality compared to other solution methods and commercial applications for target predictions.

However, depending on the boundary conditions and geometrical properties used, the results may show errors, since the method cannot consider certain acoustic effects, e.g. diffraction or multiple reflections (for details see [9]).

First calculations with an AVX512 variant of the method, which supports the processing of 16 floating point values per machine instruction, show a further performance advantage of about 25 to 50% compared to the AVX2 variant.

The next step is to test the suitability of the method as a preconditioner for iterative solvers, also when using variable reflection coefficients (shell layers).

Furthermore, it will be investigated whether the other implemented methods, such as the MLFMM or the ray tracing method, can also be optimized by AVX-based adaptations.

Porting the method to GPU HPC systems, which have significantly more computational power due to their large number of computational cores, will also be investigated, e.g., to enable a form of "real-time simulation".

PROJECT PARTNER

This project is supported by the Bundeswehr Technical Center for Ships and Naval Weapons, Maritime Technology and Research (WTD71), Eckernförde, Germany.

REFERENCES

[1] **R. J. Urick**, Principles of underwater sound, McGraw-Hill, 1967.

[2] **I. Schäfer and B. Nolte**, "Berechnung der akustischen Rückstreustärke von Unterwasserobjekten mit Hilfe der Randelementmethode und der Kirchhoffschen Hochfrequenznäherung," in *Proceedings of DAGA 2008*, Dresden, Germany, 2008.

[3] **Wikipedia**, "Advanced Vector Extensions (AVX)," [Online]. Available: https://de.wikipedia.org/wiki/Advanced_Vector_Extensions.

[4] **B. Nolte, I. Schäfer, C. de Jong and L. Gilroy**, "BeTSSi II Benchmark on Target Strength Simulation," in *Proceedings of Forum Acousticum 2014*, Krakow, Poland, 2014.

[5] **L. Brekhovskikh**, Waves in Layered Media, Academic Press, 1976.

[6] **R. Burgschweiger, I. Schäfer and M. Ochmann**, "A Multi-Level Fast Multipole Algorithm (MLFMM) for calculating the Sound scattered from Objects within Fluids," in *Proceedings of the 20th International Congress on Acoustics (ICA 2010)*, Sydney, Australia, 2010.

[7] **B. Nolte, I. Schäfer, M. Ochmann, R. Burgschweiger and S. Marburg**, "Numerical methods for wave scattering phenomena by means of different boundary formulations," *Journal of Computational Acoustics,* vol. 14, no. 4, pp. 495-529, 2008.

[8] **R. Burgschweiger, I. Schäfer, M. Ochmann and B. Nolte**, "BEAM: A ray-tracing based solver for the approximate determination of acoustic backscattering of thin-walled objects - Basics and Implementation," in *Proceedings of Forum Acousticum*, Krakow, Poland, 2014.

[9] **I. Schäfer, R. Burgschweiger, D. Sachau and J. Ehrlich**, "Hochperformante Berechnung der akustischen Rückstreustärke auf Basis der Kirchhoffschen Hochfrequenznäherung - Grundlagen," in *Proceedings of DAGA 2023*, Hamburg, Germany, 2023.